

Supplementary Information

Aminothiazole-derived N, S, Fe-doped Graphene Nanosheets as High Performance Electrocatalyst for Oxygen Reduction

Chi Chen,^{a,b} Xiao-Dong Yang,^b Zhi-You Zhou,^{*b} Yu-Jiao Lai,^b Muhammad Rauf,^b Ying Wang,^c Jing Pan,^c Lin Zhuang,^{*c} Qiang Wang,^b Yu-Cheng Wang,^b Na Tian,^b Xin-Sheng Zhang,^a and Shi-Gang Sun^{*b}

^a State Key Laboratory of Chemical Engineering, College of Chemical Engineering, East China University of Science and Technology, Shanghai, 200237, China

^b State Key Laboratory of Physical Chemistry of Solid Surfaces, Collaborative innovation center of Chemistry for Energy Materials, College of Chemistry and Chemical Engineering, Xiamen University, Xiamen, 361005, China.

^c College of Chemistry and Molecular Sciences, Hubei Key Lab of Electrochemical Power Sources, Wuhan University, Wuhan 430072, China

**Corresponding author Email: zhouzy@xmu.edu.cn; lzhuang@whu.edu.cn;
sgsun@xmu.edu.cn;*

1. Materials and methods

Catalyst preparation and characterization

AT-Fe/N/C was synthesized as following procedures. Acid-pretreated KJ600 (0.25 g) and 2-aminothiazole (2-AT, 1.5 g) were dispersed in 50 ml water by sonication. To the suspension, NaClO (8%, 15 ml) solution was added dropwise. Then the suspension was transferred into a 100 ml autoclave and performed solvothermal synthesis at 110 °C for 36 h. Under this condition, 2-AT was oxidized into poly-AT and coated on carbon black. Then FeCl₃ (1 M, 10 ml) solution was added into the above suspension. After evaporating the solvent and completely drying, the acquired solid was grinded into powder, and was subjected to heat treatment at 900 °C in Ar atmosphere for 1 h. The heat-treated sample was then pre-leached in 1 M HCl at 80 °C for 7 hours to remove unstable and inactive species from the catalyst, and thoroughly washed in de-ionized water. Finally, the catalyst was heat-treated again in Ar at 900 °C for 3 h. AT-Fe/N/SiO₂ sample was obtained from the precursor with SiO₂ nanoparticles instead of carbon black. AT/N/C catalyst was synthesized from the precursor without adding FeCl₃. Other synthetic conditions were same with those for AT-Fe/N/C.

X-ray photoelectron spectroscopy (XPS, Qtac-100 LEISS-XPS instrument), transmission electron microscope (TEM, Philips-FEI TECNAI F20 at 200 kV) were performed to characterize the composition and morphology of the AT-Fe/N/C catalyst.

Electrochemical and fuel cell tests

ORR performance was tested on a rotating ring-disk electrode (RRDE) system (Pine Inc.) with a CHI-760D bipotentiostat. Rotating speed was fixed at 900 rpm. The working electrode was prepared by dropping catalyst ink onto a glassy carbon (GC, $\phi = 5.61$ mm) disk with Pt ring. A graphite plate and a Hg/HgO electrode were used as the counter electrode and reference electrode, respectively. The potential was quoted relative to reversible hydrogen electrode (RHE) scale. The potential difference between the Hg/HgO electrode and RHE was determined to be 0.918 V.

Anion exchange membrane fuel cell (AEMFC) test: Membrane electrode assembly (MEA) with an active area of 4 cm^2 was prepared by CCM method. The home-made *a*QAPS-S₈ anion polymer electrolyte (APE) membrane ($50\ \mu\text{ m}$ in thickness) and solution were used. Cathode catalyst was AT-Fe/N/C (4 mg cm^{-2}) and anode catalyst was 80 wt% Pt/C (0.4 mg Pt cm^{-2}). Polarization curves and power density plots were recorded on Model 850e fuel cell test system (Scribner Associates Inc.) at $60\text{ }^\circ\text{C}$, under H₂/O₂ operation with the flow rate of 0.25 slpm, 100% RH and 1 bar backpressure.

Proton exchange membrane fuel cell (PEMFC) test: MEA was prepared through hot-pressing method. The catalyst “ink” was prepared by ultrasonic dispersion of AT-Fe/N/C catalyst (26 mg), 5 wt% Nafion solution (600 μl) into 1.0 ml deionized water for 1 hour. The ink was directly coated on PTFE-pretreated Toray 060 carbon paper as cathode. The loading of AT-Fe/N/C catalysts was 4.0 mg cm^{-2} . The Nafion content in cathode catalyst layer was about 50 wt%. The anode catalyst is 40 wt% Pt/C with a loading of 0.4 mg Pt cm^{-2} . The MEA was prepared by hot-pressing cathode, anode, NRE 211 Nafion membrane, and gasket at $\sim 3\text{ MPa}$ for 135 s. Fuel cell performance was tested at $80\text{ }^\circ\text{C}$ with H₂ and O₂ flow rates of 0.2 slpm at 100% RH and 1 bar back pressure.

2. Thickness characterization of graphene nanosheets

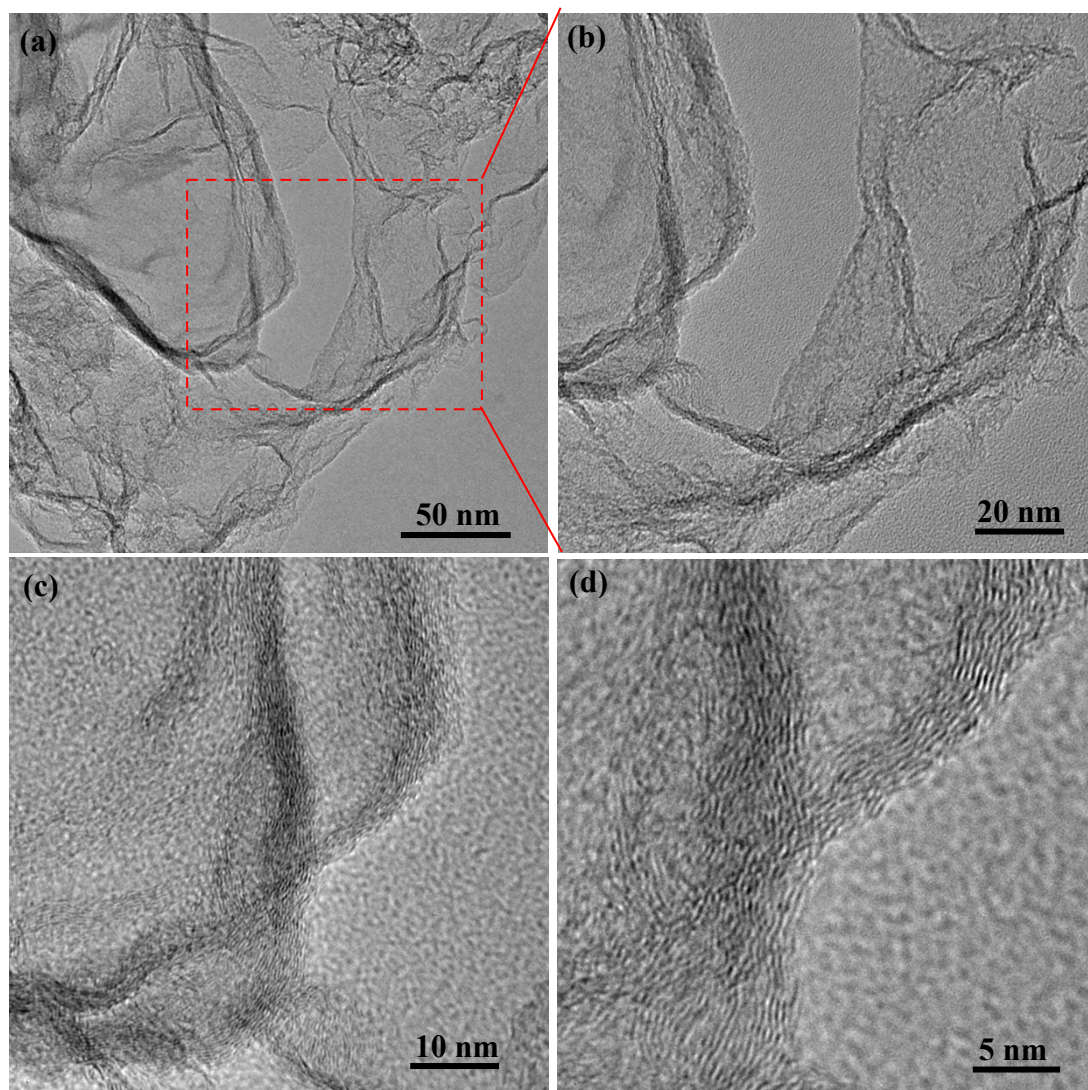


Fig. S1. TEM image of AT-Fe/N/C at the same region with increasing magnification.

The thickness of graphene nanosheets was determined to be 3–5 nm. In addition, the lattice of graphene nanosheets is not very continuous, indicating that the graphene nanosheets are not ordered and contain many defects.

3. Nitrogen adsorption/desorption isotherm

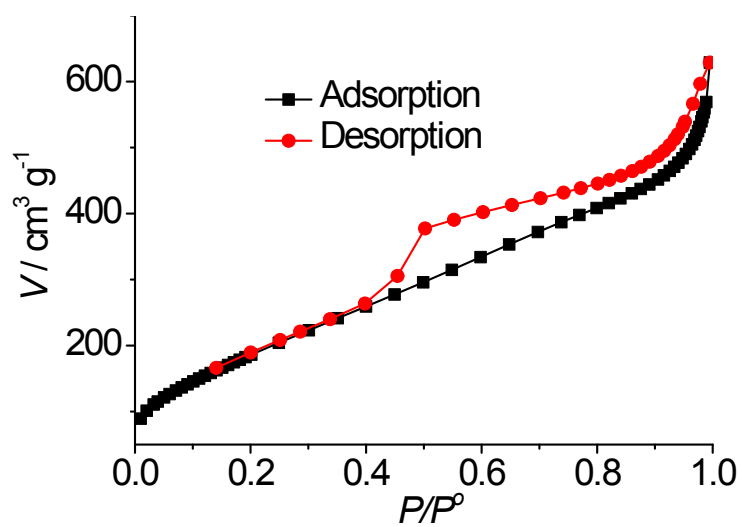


Fig. S2. Nitrogen adsorption/desorption isotherm of AT-Fe/N/C catalyst. BET surface was determined to be $708 \text{ m}^2 \text{ g}^{-1}$. The remarkable hysteresis in the medium- and high-pressure ($P/P_0 = 0.4-1$) regions between adsorption and desorption branches indicates that the catalyst contains abundant mesoporous structure.

4. High-resolution XPS of S 2p and Fe 2p

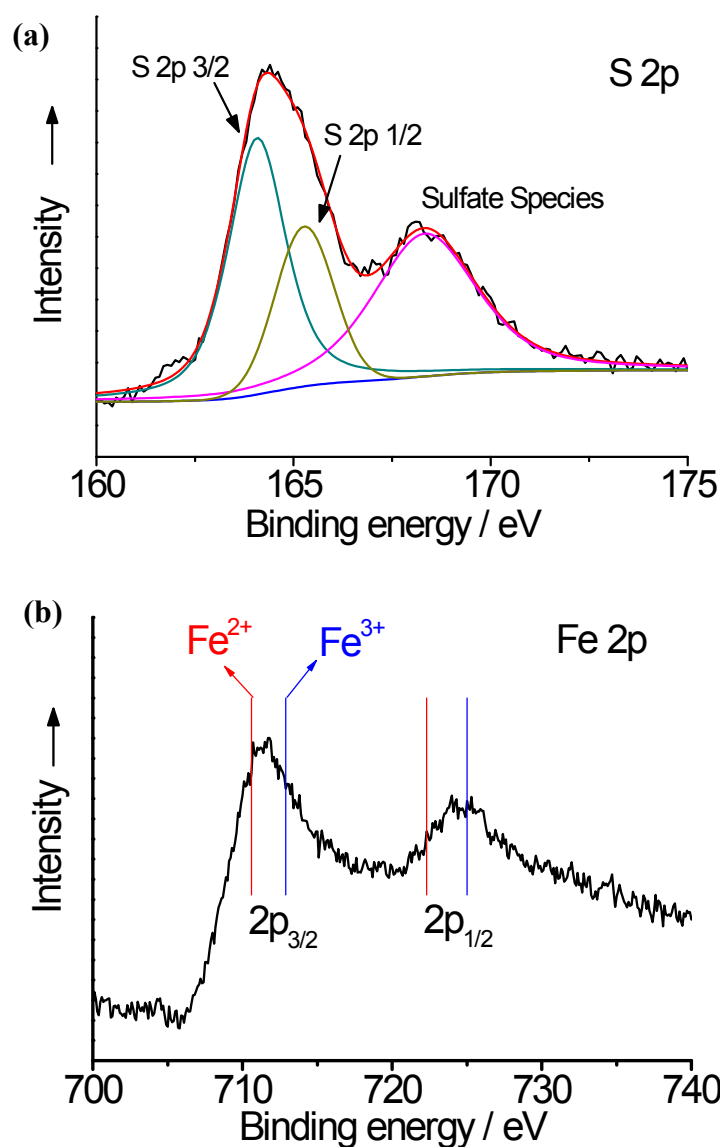


Fig. S3. (a) High-resolution XPS of S 2p of AT-Fe/N/C catalyst with the peak deconvoluted into three peaks. (b) High-resolution XPS of Fe 2p.

In the high-resolution XPS of S 2p (Fig. S3a), the intensity ratio of two peaks at 164.0 and 165.2 eV was 2:1, which were correspond to S 2p_{3/2} and S 2p_{1/2} of C-S-C species in the thiophene-like structure in graphene nanosheets. The peak at 168.3 eV was associated with C-SO_x-C species induced during heat-treatment.

In the high-resolution XPS of Fe 2p (Fig. S3b), both Fe²⁺ and Fe³⁺ exist on the AT-Fe/N/C as detected by XPS (Fig. A4). Note that, under electrochemical ORR conditions, the value states of Fe element may change depending on electrode potential.

5. Raman spectroscopy

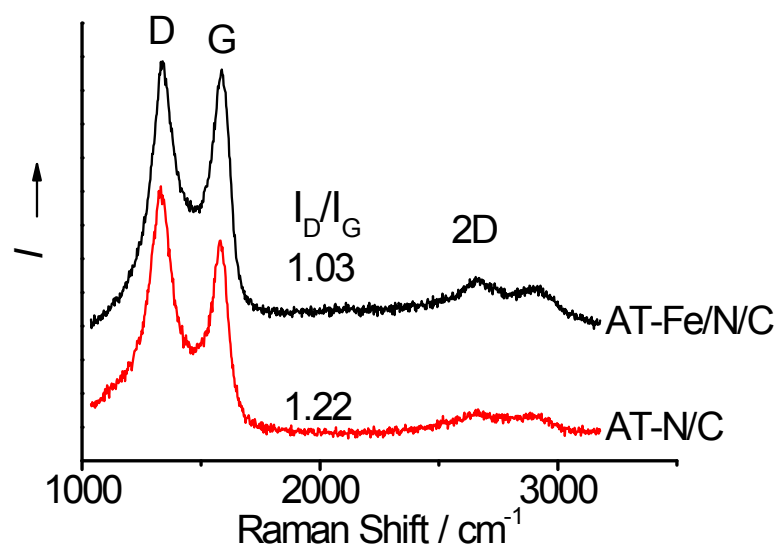


Fig. S4. Raman spectra of AT-Fe/N/C and AT-N/C.

The Raman spectroscopy was carried out to evaluate the defects of AT-Fe/N/C. As a control sample, AT-N/C, which does not contain graphene structure, was also tested. As shown in Fig. S4, typical D and G bands, locating at around 1330 and 1580 cm⁻¹, respectively, can be observed. The intensity ratio of D band to G band (I_D/I_G) of AT-Fe/N/C and AT-N/C are 1.03 and 1.22, respectively. The lower I_D/I_G ratio of AT-Fe/N/C can be attributed to higher graphitic degree as compared with AT-N/C. Nevertheless, the I_G is still slightly lower than the I_D on the AT-Fe/N/C (the co-existence of carbon black nanoparticles can also contribute to high level of D band), suggesting the high concentration of defects on the graphene nanosheets. This may be ascribed to the high level of heteroatom doping into the graphene framework, and is also consistent with the HRTEM result (Fig. S1).

6. Comparison of CV characteristic before and after the durability test

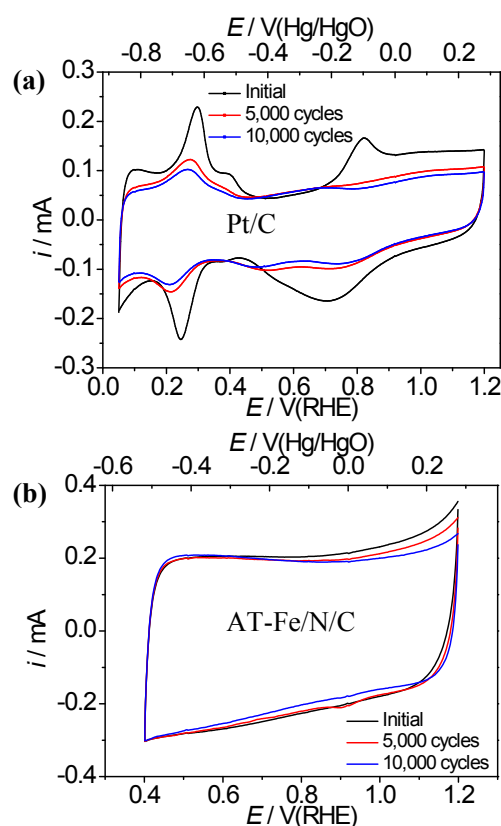


Fig. S5. Cyclic voltammograms of (a) Pt/C catalyst (0.1 mg cm^{-2}) and (b) AT-Fe/N/C catalyst (1.0 mg cm^{-2}) recorded in N_2 -saturated 0.1 M NaOH before and after the accelerated durability test by 10,000 potential cycling. Note that the accelerated durability test was conducted in O_2 -saturated solution.

For Pt/C, the electrochemically active area were 2.56 , 1.12 and 0.87 cm^2 before the accelerated durability test, after 5,000 and 10,000 potential cycles, respectively. The loss of electrochemically active area is mostly caused by the aggregation and dissolution of Pt nanoparticles. After 10,000 potential cycles, the electrochemically active area of Pt/C remained 34% of that of initial. As comparison, the CV curves of AT-Fe/N/C catalyst remain almost unchanged. The slightly decrease of current in high potential region may be related to loss of oxidizable carbon and impurity.

7. Methanol tolerance

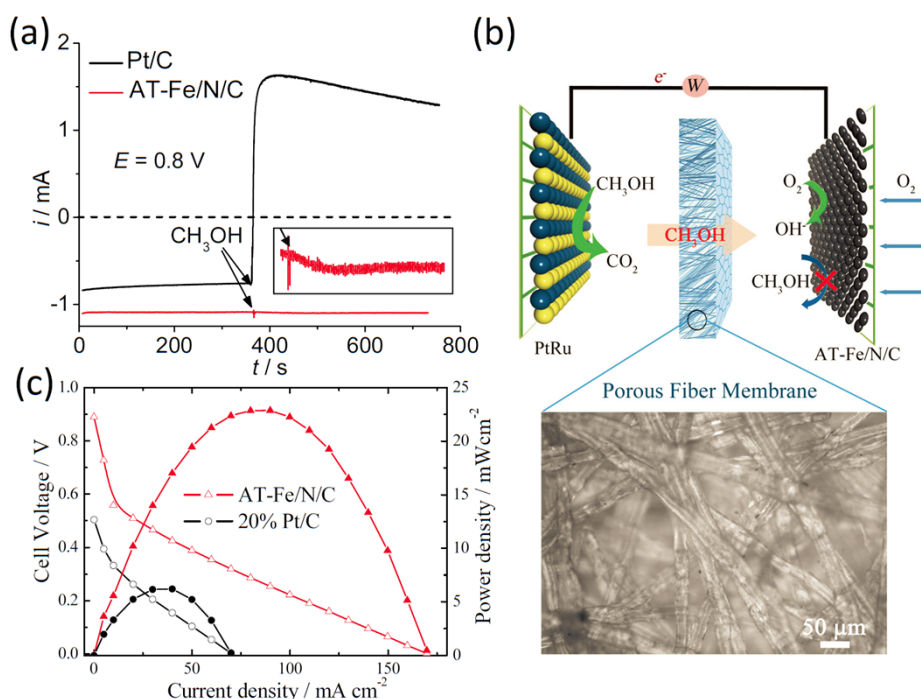


Fig. S6. (a) Methanol tolerance of AT-Fe/N/C and Pt/C catalysts at 0.8 V in O_2 -saturated 0.1 M NaOH. The inset shows the enlarged curves of AT-Fe/N/C catalyst after methanol injection. (b) Illustration of DMFC using porous polypropylene fiber separator as membrane, PtRu/C as anode catalyst and AT-Fe/N/C as cathode catalyst. Methanol can cross over freely through this porous membrane. (c) The performance of fiber membrane-based DMFC using AT-Fe/N/C (4 mg cm^{-2}) or Pt/C (20 wt%, 4 mg cm^{-2}) as cathode catalysts at room temperature. Anode catalyst: PtRu/C (60 wt%, 5 mg cm^{-2}); Anode was fed with 3 M methanol + 2 M NaOH. A porous polypropylene fiber membrane was used, seeing photomicrograph in b).

The AT-Fe/N/C catalyst exhibits high tolerance to methanol. After the injection of methanol into electrolyte solution to reach a concentration of 0.5 M, the ORR current of AT-Fe/N/C changed little (Fig. S6a). In the enlarged figure (inset to Fig. S6a), we can observe that the ORR current was even increased slightly, which may be related to the increase of O_2 solubility in water-methanol mixed solution. In contrast, the current of Pt/C dramatically changed from a negative value for ORR to a positive value for methanol oxidation after methanol injection.

The high methanol tolerance enables the AT-Fe/N/C to be applied in DMFC using porous fiber membrane instead of ion-exchanged membrane. The fiber membrane has very low-cost, but freely permeable for methanol. We built a DMFC using a polypropylene fiber separator as membrane, AT-Fe/N/C as cathode catalyst and PtRu/C as anode catalyst (Fig. S6b). The DMFC exhibits peak power density of 23 mW cm^{-2} operated at room temperature (Fig. S6c). However, the Pt/C cathode cannot work in this configuration due to severe crossover of methanol, and the peak power density is very low (6 mW cm^{-2}).

Table S1. Comparison of ORR activity of the NPM catalysts in alkaline medium reported in literatures.

Catalyst	Electrolyte	Loading / mg cm ⁻²	Rotating Speed / rpm	E _{1/2} / V vs RHE	Mass activity at 0.95V (A g ⁻¹)	Mass activity at 1.0 V (A g ⁻¹)	Ref.
AT-Fe/N/C	0.1 M NaOH	0.60	900	0.926	3.08	0.56	This work
NT-G	0.1 M KOH	0.485	1600	0.875	1.58	0.42	[1]
N-Fe- CNT/CNP	0.1 M NaOH	1.0	900	0.93	1.89	0.39	[2]
CNT/HDC- 1000	0.1 M KOH	0.6	1600	0.82	0.18	/	[3]
Fe3C/C-800	0.1 M KOH	0.6	900	0.83	0.21	/	[4]
BP2000-NF	0.1 M KOH	0.39	1600	0.88	1.68	/	[5]
NDCN-22	0.1 M KOH	0.6	1600	0.836	0.66	/	[6]
Fe-NG-30	0.1 M KOH	0.4	900	0.89	1.32	/	[7]
A-NPC	0.1 M KOH	0.127	1600	0.809	0.97	/	[8]
N-CNT/N-G	0.1 M KOH	0.6	1600	0.84	0.30	/	[9]
Fe/NG/C	0.1 M KOH	0.5	1600	0.879	1.63	0.49	[10]
BP-NFe	0.1 M KOH	0.4	1600	0.911	3.61	0.40	[11]
(DFTPP)Fe- lm-CNTs	0.1 M KOH	1.0	1600	0.922	4.18	1.53	[12]
FePc-Py-CNT	0.1 M KOH	0.318	1600	0.917	2.74	/	[13]
S/N_Fe27	0.1 M KOH	0.8	1500	0.875	0.68	/	[14]
P-Fe-N-CNF	0.1 M KOH	0.2	1600	0.84	0.94	/	[15]
Fe-N-CNT- OPC	0.1 M KOH	0.4	1600	0.825	0.64	/	[16]

Hg/HgO electrode, Ag/AgCl electrode and SCE were converted into RHE scale. $E(\text{RHE}) = E(\text{Hg}/\text{HgO}) + 0.918 \text{ V}$, $E(\text{RHE}) = E(\text{Ag}/\text{AgCl}) + 0.966 \text{ V}$, $E(\text{RHE}) = E(\text{SCE}) + 1.002 \text{ V}$. These conversion values were experimentally measured, that is, the open-circuit potential between a reference electrode of Hg/HgO (or Ag/AgCl, or SCE) and RHE electrode (i.e., a Pt black electrode in H₂-saturated 0.1 M NaOH solution)

Kinetic current was calculated by correction of diffusion-limited current. The absolute current and diffusion limiting current were read from ORR polarization curves. In some cases, the absolute current at 1.0 V was immeasurable.

References for Table S1

1. Y. Li, W. Zhou, H. Wang, L. Xie, Y. Liang, F. Wei, J. C. Idrobo, S. J. Pennycook and H. Dai, *Nat. Nanotech.*, 2012, **7**, 394-400.
2. H. T. Chung, J. H. Won and P. Zelenay, *Nat. commun.*, 2013, **4**, 1922-1926.

3. Y. J. Sa, C. Park, H. Y. Jeong, S. H. Park, Z. Lee, K. T. Kim, G. G. Park and S. H. Joo, *Angew. Chem. Int. Ed.*, 2014, **53**, 4102-4106.
4. Y. Hu, J. O. Jensen, W. Zhang, L. N. Cleemann, W. Xing, N. J. Bjerrum and Q. Li, *Angew. Chem. Int. Ed.*, 2014, **53**, 3675-3679.
5. X. Sun, P. Song, Y. Zhang, C. Liu, W. Xu and W. Xing, *Sci. Rep.*, 2013, **3**, 2505-2509.
6. W. Wei, H. Liang, K. Parvez, X. Zhuang, X. Feng and K. Mullen, *Angew. Chem. Int. Ed.*, 2014, **53**, 1570-1574.
7. B. J. Kim, D. U. Lee, J. Wu, D. Higgins, A. Yu and Z. Chen, *J. Phys. Chem. C*, 2013, **117**, 26501-26508.
8. S. Zhang, M. S. Miran, A. Ikoma, K. Dokko and M. Watanabe, *J. Am. Chem. Soc.*, 2014, **136**, 1690-1693.
9. S. Zhang, H. Zhang, Q. Liu and S. Chen, *J. Mater. Chem. A*, 2013, **1**, 3302-3308.
10. Q. Liu, H. Zhang, H. Zhong, S. Zhang and S. Chen, *Electrochim. Acta*, 2012, **81**, 313-320.
11. J. Liu, X. Sun, P. Song, Y. Zhang, W. Xing and W. Xu, *Adv. Mater.*, 2013, **25**, 6879-6883.
12. P. J. Wei, G. Q. Yu, Y. Naruta and J. G. Liu, *Angew. Chem. Int. Ed.*, 2014, **53**, 6659-6663.
13. R. Cao, R. Thapa, H. Kim, X. Xu, M. Gyu Kim, Q. Li, N. Park, M. Liu and J. Cho, *Nat. Commun.*, 2013, **4**, 2076-2082.
14. N. Ranjbar Sahraie, J. P. Paraknowitsch, C. Gobel, A. Thomas and P. Strasser, *J. Am. Chem. Soc.*, 2014, **136**, 14486-14497.
15. B. Jeong, D. Shin, H. Jeon, J. D. Ocon, B. S. Mun, J. Baik, H. J. Shin and J. Lee, *ChemSusChem*, 2014, **7**, 1289-1294.
16. J. Liang, R. F. Zhou, X. M. Chen, Y. H. Tang and S. Z. Qiao, *Adv. Mater.*, 2014, **26**, 6074-6079.

Table S2. Performance comparison of alkaline anion exchange membrane fuel cells (AEMFCs) employing NPM catalyst as the cathode.

Catalyst	Operation Temperature / °C	Cathode Loading / mg cm ⁻²	Peak Power Density / mW cm ⁻²	Ref.
AT-Fe/N/C	60	4	164	This work
CNT/HDC-1000	50	2	270	[1]
BP _{ox} -NFe	50	2	107	[2]
N-CNT	50	5	37	[3]
NCNHs	50	3	30	[4]
NpGr-72	50	2.5	27	[5]
Py-CoPc/C	RT	1.5	21	[6]
CuPc/C	RT	3.6	6.8	[7]

References for Table S2

1. Y. J. Sa, C. Park, H. Y. Jeong, S. H. Park, Z. Lee, K. T. Kim, G. G. Park and S. H. Joo, *Angew. Chem. Int. Ed.*, 2014, **53**, 4102-4106.
2. P. Song, Y. W. Zhang, J. Pan, L. Zhuang and W. L. Xu, *Chem. Commun.* 2015, **51**, 1972-1975.
3. C. V. Rao and Y. Ishikawa, *J. Phys. Chem. C* 2012, **116**, 4340-4346.
4. S. M. Unni, S. N. Bhange, R. Illathvalappil, N. Mutneja, K. R. Patil and S. Kurungot, *Small*, 2015, **11**, 352-360.
5. T. Palaniselvam, M. O. Valappil, R. Illathvalappil and S. Kurungot, *Energ. Environ. Sci.*, 2014, **7**, 1059-1067.
6. X. F. Dai, M. F. Zhen, P. Xu, J. J. Shi, C. Y. Ma and J. L. Qiao, *Acta Phy-Chim. Sin.*, 2013, **29**, 1753-1761.
7. L. Ding, Q. Xin, X. F. Dai, J. Zhang and J. L. Qiao, *Ionics*, 2013, **19**, 1415-1422.

Table S3. Durability comparison of NPM catalysts for ORR in alkaline media reported in literatures.

Catalyst	Electrolyte	Potential / V (RHE)	Duration / h	Current Retention / %	Ref.
AT-Fe/N/C	0.1 M NaOH	0.80	15 25 100	97 96 91	This work
B,N-graphene	0.1 M KOH	0.67	85	82	[1]
Fe ₃ C/C-800	0.1 M KOH	0.80	14	70	[2]
(DFTPP)Fe-Im-CNTs	0.1 M KOH	0.70	25	95	[3]
CNF@NG	0.1 M KOH	0.40	10	90	[4]
150-C/CN	0.1 M KOH	0.67	60	80	[5]
Carbon-L	0.1 M KOH	0.60	7	75	[6]
N-S-G	0.1 M KOH	0.72	60	81	[7]
Ar-800	0.1 M KOH	0.72	5.6	62	[8]
NOSC8-900	0.1 M KOH	0.45	12.5	93	[9]
Fe-N-CNT-OPC	0.1 M KOH	0.67	5.6	93	[10]

References for Table S3

1. Y. Zheng, Y. Jiao, L. Ge, M. Jaroniec and S. Z. Qiao, *Angew. Chem. Int. Ed.*, 2013, **52**, 3110-3116.
2. Y. Hu, J. O. Jensen, W. Zhang, L. N. Cleemann, W. Xing, N. J. Bjerrum and Q. Li, *Angew. Chem. Int. Ed.*, 2014, **53**, 3675-3679.
3. P. J. Wei, G. Q. Yu, Y. Naruta and J. G. Liu, *Angew. Chem. Int. Ed.*, 2014, **53**, 6659-6663.
4. T. N. Ye, L. B. Lv, X. H. Li, M. Xu and J. S. Chen, *Angew. Chem. Int. Ed.*, 2014, **53**, 6905-6909.
5. J. Liang, Y. Zheng, J. Chen, J. Liu, D. Hulicova-Jurcakova, M. Jaroniec and S. Z. Qiao, *Angew. Chem. Int. Ed.*, 2012, **51**, 3892-3896.
6. P. Zhang, F. Sun, Z. Xiang, Z. Shen, J. Yun and D. Cao, *Energ. Environ. Sci.*, 2014, **7**, 442-450.
7. J. Liang, Y. Jiao, M. Jaroniec and S. Z. Qiao, *Angew. Chem. Int. Ed.*, 2012, **51**, 11496-11500.
8. J. S. Lee, G. S. Park, S. T. Kim, M. Liu and J. Cho, *Angew. Chem. Int. Ed.*, 2013, **125**, 1060-1064.
9. Y. Meng, D. Voiry, A. Goswami, X. Zou, X. Huang, M. Chhowalla, Z. Liu and T. Asefa, *J. Am. Chem. Soc.*, 2014, **136**, 13554-13557.
10. J. Liang, R. F. Zhou, X. M. Chen, Y. H. Tang and S. Z. Qiao, *Adv Mater*, 2014, **26**, 6074-6079.